MedChemComm

RSC Publishing

CONCISE ARTICLE

View Article Online
View Journal

Berberine azoles as antimicrobial agents: synthesis, biological evaluation and their interactions with human serum albumin†

Cite this: DOI: 10.1039/c3md00032j

Shao-Lin Zhang, Juan-Juan Chang, Guri L. V. Damu,‡ Rong-Xia Geng* and Cheng-He Zhou*

A series of berberine azoles was synthesized and characterized by NMR, IR, MS and HRMS spectroscopy. All the newly prepared compounds were screened for their antimicrobial activities. Bioactivity assays manifested that most of the berberine azoles exhibited good antimicrobial activities. Especially compound **7a** displayed remarkable anti-*Proteus vulgaris* and anti-*Candida mycoderma* efficacies, which were comparable to or even better than for the reference drugs. The binding behavior of compound **7a** to human serum albumin (HSA) revealed that hydrophobic interactions and hydrogen bonds play important roles in the association of compound **7a** with HSA. Molecular docking experiments showed that compound **7a** has moderate affinity to HSA, and the theoretical calculations were in accordance with the experimental results.

Received 29th January 2013
Accepted 10th March 2013

DOI: 10.1039/c3md00032j

www.rsc.org/medchemcomm

1 Introduction

Azole compounds are an important class of nitrogen-containing heterocycles with desirable electron-rich properties. This type of special structure endows azole derivatives with the ability to readily bind to enzymes and receptors in biological systems *via* noncovalent interactions such as hydrogen bonds, coordination bonds, ion–dipole, cation–π, π–π stacking, hydrophobic effects and van der Waals forces. Thereby they exhibit various bioactivities, such as antifungal,[1–5] antibacterial,[6–10] anticancer,[11,12] antitubercular,[13] antiviral,[14] antiproliferative,[15] anticonvulsant,[16] antiparasitic,[17] antihistaminic,[18] antihypertensive[19] and other effects. Especially in antimicrobial applications,[20] azole compounds have been extensively investigated as antibacterial and antifungal drugs and some of them, such as clotrimazole, miconazole, tioconazole, terconazole, itraconazole and fluconazole have been employed in the clinic to treat various types of microorganism infections. One of the most significant achievements is the successful exploitation of fluconazole, which has established an exceptional therapeutic record for *candida* infections, and has become the first choice for the treatment of antifungal infections due to its potent activities, excellent safety profiles and favorable pharmacokinetic characteristics. However, with increasing misuse and the abuse of azole-based drugs, more and more bacterial and fungal strains have become resistant to these agents. Thus, these trends have facilitated the urgent need to develop more effective and safe antimicrobial agents. Among the attractive approaches to achieve this goal, structural modification of fluconazole in order to broaden its antimicrobial spectrum and increase therapeutic indexes has provoked special interest in the realm of medicinal chemistry. In our previously reported work,[6] we developed new structural analogues of fluconazole, in which the tertiary alcohol was replaced by a tertiary amino group, and the methylene bridge between the tertiary alcohol and the triazolyl moieties was substituted by an ethylene chain. Bioactive evaluation manifested that these types of fluconazole analogues exhibited good antibacterial and antifungal activities which were comparable to or even better than for the reference drugs chloromycin, norfloxacin and fluconazole, showing their great potential and development value. Therefore, we have interest in further investigating this type of new frame.

As is known to us, berberine is a well-known natural isoquinoline alkaloid which has been demonstrated to possess a variety of pharmacological activities such as antimicrobial,[21] antineoplastic,[22] antiviral,[23] antiinflammatory,[24] antiprotozoal,[25] and antileishmanial[26] effects. Especially as an antimicrobial agent, berberine has been playing significant roles in the clinic for the treatment of infectious diseases such as acute gastroenteritis, cholera and bacillary dysentery. This overwhelmingly compels us with great interest to develop berberine-based antimicrobial agents.

School of Chemistry and Chemical Engineering, Southwest University, Chongqing 400715, People's Republic of China. E-mail: geng0712@swu.edu.cn; zhouch@swu.edu.cn; Fax: +86-23-68254967; Tel: +86-23-68254967

† Electronic supplementary information (ESI) available: Experimental procedures for the prepared compounds and bioassay procedures; spectral data of the prepared compounds. See DOI: 10.1039/c3md00032j

‡ Postdoctoral fellow from Indian Institute of Chemical Technology (IICT), Hyderabad-500 607, India.

In view of this, we combined berberine and the tertiary amino frame to afford a series of hybrids as a new type of fluconazole analogues, which were expected to increase their bioactivities and extend their antimicrobial spectrum. Moreover, various azole rings including 1,2,4-triazole, benzotriazole, imidazole, benzimidazole, 2-mercaptobenzimidazole and 5,6-dimethyl-benzimidazole were incorporated into our target compounds to explore their contributions to the antimicrobial activities. Further binding behaviors between the synthesized compound and human serum albumin (HSA) were investigated to preliminarily evaluate their transportation and pharmacokinetic properties. It is well accepted that the overall distribution, metabolism, and efficacies of drugs can be modified by their affinity to HSA,[27,28] and many promising new drugs have been rendered ineffective because of their unusually high affinity to this protein.[29] Full investigations of interactions between drugs or bioactive small molecules and HSA are not only beneficial for providing a deeper understanding of the absorption, transportation, distribution, metabolism and excretion properties of drugs, but are also significant to the design, modification and screening of drug molecules. In this work, information on interactions between HSA and a target compound with high antimicrobial activities was obtained by fluorescence and UV-vis absorption spectroscopy on a molecular level. Finally, molecular docking experiments were employed to reconfirm the interaction behaviors between the prepared compound and HSA.

2 Chemistry

The synthetic routes to the target berberine azoles were outlined in Schemes 1 and 2. The target berberine azole compounds were prepared starting from halobenzyl halides **3a–h**. The *N*-alkylation of diethanolamine with a series of halobenzyl halides **3a–h** produced the intermediates **4a–h** in excellent yields of 92.3–98.6%, and then the latter were brominated in chloroform with phosphorus tribromide to afford the dibromides **5a–h** according to procedures similar to our previous work.[6] Subsequently, compounds **5a–h** were reacted with 1,2,4-triazole, benzotriazole, imidazole, benzimidazole, 2-mercaptobenzimidazole and 5,6-dimethyl-benzimidazole through *N*-alkylation to conveniently afford the corresponding mono-triazoles **6a–h**, mono-imidazole **8**, mono-benzimidazoles **10a–c** and mono-benzotriazole **12**. Finally, these mono-azoles were coupled with the berberrubine **2** to afford the desired target berberine-derived triazoles **7a–h**, imidazole compound **9**, benzimidazoles **11a–c** and benzotriazole derivative **13**. All the newly synthesized compounds were characterized by NMR, IR, MS and HRMS spectra (ESI 1†).

3 Results and discussion

3.1 Antimicrobial activities

The tested antimicrobial results (ESI 2†) in Table 1 revealed that most of the prepared berberine azoles **7a–h**, **9**, **11a–c** and **13** inhibit the growth of Gram-positive bacteria, Gram-negative bacteria and fungi, to a superior amount compared to their precursors **6a–h**, **8**, **10a–c** and **12**. Notably, the berberine triazole **7a** gave the best antimicrobial activities (MIC = 2–8 μg mL^{-1}), which were comparable to or even better than the reference drugs. This result suggests that the incorporation of the berberine moiety into the target compounds was favorable for the enhancement of antimicrobial activities.

For the tested berberine triazoles **7a–h**, all compounds showed good inhibitory efficacy at concentrations of 2–32 μg mL^{-1} against the tested strains. Particularly, compound **7a** was the most active one and displayed remarkable antimicrobial activities, especially for *proteus vulgaris* (MIC = 2 μg mL^{-1}), which was 4-, 16- and 64-fold more potent than the reference drugs norfloxacin, chloromycin and berberine. Notably, compounds **7a** and **7f–h** have a low inhibitory concentration (MIC = 8 μg mL^{-1}) against *MRSA*, which makes them 2- and 16-fold more potent than the reference drugs chloromycin and berberine, respectively, and equipotent to norfloxacin. This indicated that this type of compounds could be employed to further study as potent novel anti-*MRSA* agents.

Berberine benzimidazoles **11a–b** and **13** showed weaker activities than berberine triazoles **7a–h**, but compound **11b**, bearing an electron donating methyl group, displayed good anti-*shigella dysenteriae* activity with an MIC value of 4 μg mL^{-1}, which was 8- and 64-fold more potent than that of chloromycin and berberine, respectively. Compared to berberine triazoles and imidazole, berberine benzotriazole **11c** and its precursor **10c** showed lower antimicrobial efficacies.

The above results clearly pointed out that the antimicrobial efficacies should be closely related to azolyl moieties and halobenzyl groups to some extent. For this series of compounds, azolyl moieties contributed to the antimicrobial activities in the order of triazolyl > imidazolyl > 5,6-dimethyl-benzimidazolyl > benzimidazolyl > benzotriazolyl. For berberine triazoles, dihalobenzyl groups are more helpful for increasing antimicrobial efficacies in comparison to the monohalobenzyl ones, and a difluoro-substituted derivative showed the highest antimicrobial potency.

3.2 Binding discussion

3.2.1 UV-vis absorption spectral study. UV-vis absorption measurement is a very easy operational method and applicable to explore the structural change of protein and to identify complex formation. In our binding experiment, a UV-vis absorption spectroscopic method was employed to evaluate the binding interactions between compound **7a** and HSA. As shown in Fig. 1, two absorption peaks were observed at 278 and 338 nm, respectively, and the peak intensity increased with the addition of compound **7a**. The obvious enhancement of absorbance intensity revealed the interactions between HSA and compound **7a**. This result can be explained by the change of environment of the Tryptophan (Trp-214) residue, and the slight increase in hydrophobicity of the microenvironment of the Trp-214 residue.[30]

3.2.2 Fluorescence quenching mechanism. Fluorescence spectroscopy is an effective method to study the interactions of small molecules with HSA. The fluorescence intensity of

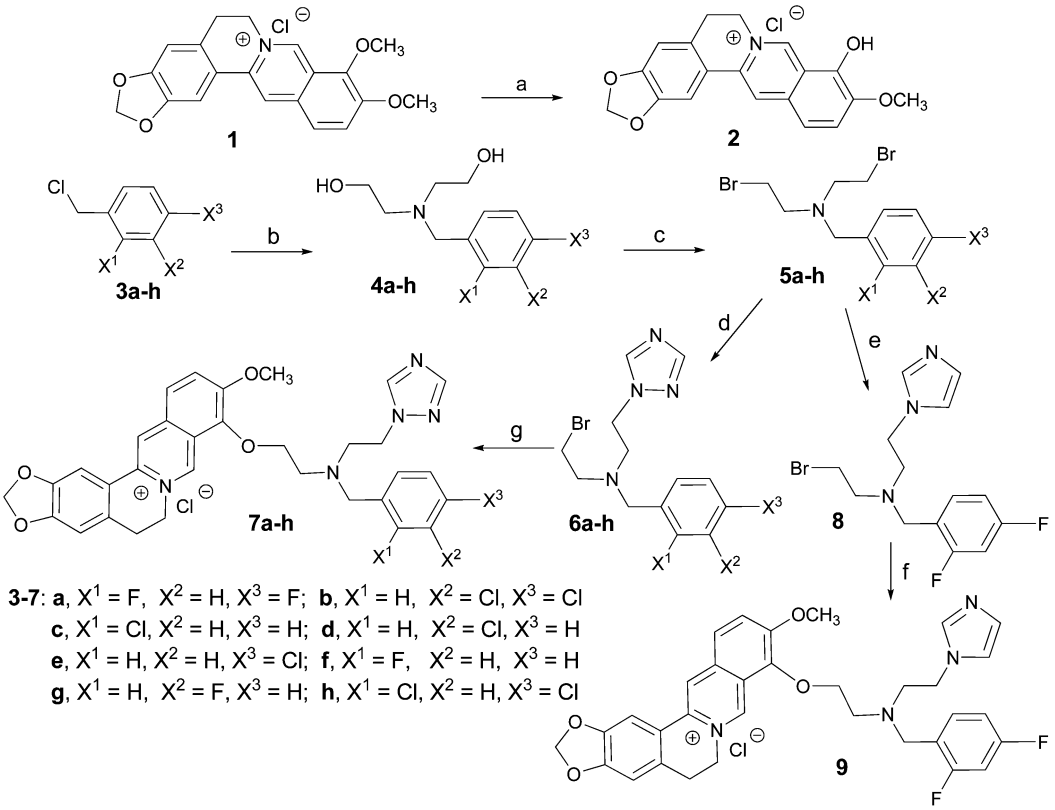

Scheme 1 Synthetic routes to berberine triazoles and imidazole. *Reagents and conditions*: (a) berberine, 20 mm Hg, 190 °C, 15 min; (b) CH_3CN, diethanolamine, 50 °C, 10–12 h, 92.3–98.6% yield; (c) $CHCl_3$, PBr_3, reflux, 2 h, 88.1–98.5% yield; (d) 1,2,4-triazole, K_2CO_3, CH_3CN, 30 °C, 12 h, 21.9–64.1% yield; (e) imidazole, NaH, THF, 60 °C, 57.3% yield ; (f) DMF, 110 °C, 20 h, 30.8% yield; (g) DMF, 110 °C, 20 h, 21.0–38.6% yield.

Trp-214 may change when HSA interacts with other small molecules, which can be seen in the fluorescence spectra of HSA in the UV region. The effect of compound **7a** on the fluorescence intensity of HSA at 298 K is shown in Fig. S1 (ESI 3†). HSA has a strong fluorescence emission with a peak at 348 nm, owing to the single Try-214 residue. The intensity of this characteristic broad emission band decreased steadily with the increase in concentration of compound **7a**, accompanied with a blue shift wavelength (from 348 to 342 nm) in the albumin spectrum. This suggests an increased hydrophobicity of the region surrounding Trp-214.[28]

The fluorescence quenching data can be analyzed by the Stern–Volmer equation:[31]

$$\frac{F_0}{F} = 1 + K_{SV}[Q] \quad (1)$$

where F_0 and F represent fluorescence intensities in the absence and presence of compound **7a**, respectively. K_{SV} is the Stern–Volmer

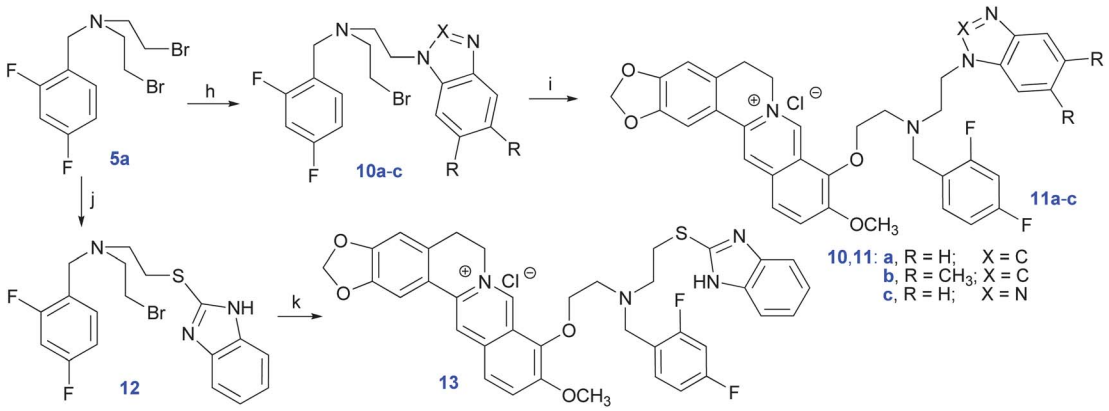

Scheme 2 Synthetic routes to berberine benzimidazoles and benzotriazole. *Reagents and conditions*: (h) CH_3CN, 60 °C, 10–12 h, 32.9–40.2% yield; (i) DMF, 110 °C, 20 h; (j) CH_3CN, 60 °C, 10–12 h, 60.0% yield; (k) DMF, 110 °C, 20 h, 33.4% yield.

Table 1 *In vitro* antimicrobial activities for the prepared compounds expressed as MIC (μg mL^{-1})[abc]

	Gram-positive bacteria				Gram-negative bacteria				Fungi			
Compds	MRSA	SA	BS	ML	EC	SD	PA	PV	CA	CM	CU	BF
6a	128	64	256	32	32	64	128	128	32	256	256	128
6b	256	64	256	32	32	128	128	256	32	256	64	128
6c	256	128	256	64	64	256	128	512	64	256	128	256
6d	256	128	256	64	128	256	256	>512	64	256	256	128
6e	256	128	256	512	128	256	256	512	128	256	128	64
6f	128	64	256	64	32	64	128	256	32	256	128	64
6g	128	64	256	64	64	64	128	256	32	256	256	128
6h	256	64	256	32	32	128	128	128	32	256	256	256
7a	8	4	8	8	4	4	8	2	4	2	8	32
7b	16	8	8	16	8	16	16	8	8	4	32	32
7c	16	8	8	32	8	32	32	16	16	8	32	16
7d	32	8	16	32	8	32	32	32	16	4	8	32
7e	16	16	8	16	16	8	16	32	32	32	16	32
7f	8	4	8	8	4	4	8	4	4	2	16	16
7g	8	8	8	16	8	4	8	4	4	4	8	16
7h	8	8	8	16	4	8	16	8	4	4	16	16
8	64	64	128	64	128	128	32	256	64	32	64	128
9	16	8	16	32	32	16	16	32	32	32	32	32
10a	256	128	256	256	512	64	128	512	128	64	128	128
10b	128	64	32	64	128	16	64	128	128	64	128	256
10c	128	256	256	256	128	64	128	256	>512	>512	256	256
11a	32	16	32	16	32	8	16	32	32	32	16	32
11b	32	32	16	16	32	4	8	8	32	16	16	16
11c	64	64	128	128	128	32	64	128	>512	>512	32	16
12	>512	>512	>512	>512	>512	>512	>512	>512	>512	>512	512	512
13	64	32	64	128	32	128	64	64	64	128	64	64
A	16	16	32	8	32	32	32	32	—	—	—	—
B	8	0.5	1	2	16	4	16	8	—	—	—	—
C	128	512	>512	>512	>512	256	256	128	>512	128	256	128
D	—	—	—	—	—	—	—	—	1	4	8	16

[a] Minimum inhibitory concentrations were determined by a micro broth dilution method for microdilution plates. [b] MRSA, Methicillin resistant *Staphylococcus aureus* N315; SA, *Staphylococcus aureus* ATCC25923; BS, *Bacillus subtilis* ATCC6633; ML, *Micrococcus luteus* ATCC 4698; EC, *Escherichia coli* DH52; SD, *Shigella dysenteriae* ATCC51252; PA, *Pseudomonas aeruginosa* ATCC27853; PV, *Proteus vulgaris* ATCC8427; CA, *Candida albicans* ATCC90029; CM, *Candida mycoderma*; CU, *Candida utilis* ATCC9950; BF, *Beer yeast* ATCC9763. [c] **A** = chloromycin; **B** = norfloxacin; **C** = berberine; **D** = fluconazole.

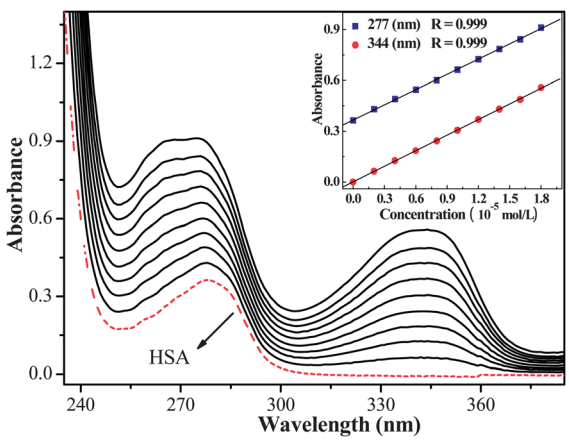

Fig. 1 Effect of compound **7a** on the UV-vis absorption of HSA, c(HSA) = 1.0 × 10^{-5} mol L^{-1}; c(compound **7a**)/(10^{-5} mol L^{-1}): 0, 0.2, 0.4, 0.6, 0.8, 1, 1.2, 1.4, 1.6, 1.8 (T = 294 K, pH = 7.40). The inset corresponds to the absorbance at 277 and 344 nm at different concentrations of compound **7a**.

quenching constant, and [Q] is the concentration of compound **7a**. The Stern–Volmer plots of HSA in the presence of compound **7a** at different concentrations and temperatures are shown in Fig. S2 (ESI 3†).

Fluorescence quenching can occur *via* different mechanisms, usually classified as dynamic quenching or static quenching depending on temperature and viscosity. Because higher temperatures result in larger diffusion coefficients, the quenching constants are expected to increase with a gradually increasing temperature in dynamic quenching. However, increasing of the temperature is likely to result in a smaller static quenching constant due to the dissociation of weakly bound complexes.

Therefore, the K_{SV} values at each temperature were calculated from Stern–Volmer plots. The result (Table 2) showed that the Stern–Volmer quenching constants were inversely correlated with temperature, which indicated that the probable quenching mechanism of the compound **7a**–HSA binding reaction was initiated by ground-state complex formation.[30]

Table 2 Stern–Volmer quenching constants for the interactions of compound **7a** with HSA at various temperatures

pH	T (K)	$10^{-4}K_{SV}$ (L mol^{-1})	R^a	S.D.^{b}
7.4	294	8.73	0.9943	0.1006
	302	7.12	0.9940	0.0799
	310	6.51	0.9948	0.0666

^{a} R is the correlation coefficient. ^{b} S.D. is the standard deviation.

In order to reconfirm that the probable quenching mechanism of fluorescence of HSA by compound **7a** was mainly initiated by ground-state complex formation, the difference in absorption spectroscopy was employed. The UV-vis absorption spectrum of HSA and the difference in the absorption spectrum between the compound **7a**–HSA complex and compound **7a** at the same concentration could not be superposed (Fig. S3, ESI 3†), this result suggests that the probable quenching mechanism of fluorescence of HSA by compound **7a** was mainly a static quenching procedure.[28]

3.2.3 Binding constant and site. For a static quenching process, the data could be described by the Modified Stern–Volmer equation:[32]

$$\frac{F_0}{\Delta F} = \frac{1}{f_a K_a}\frac{1}{[Q]} + \frac{1}{f_a} \quad (2)$$

where ΔF is the difference in fluorescence intensity in the absence and presence of compound **7a** at concentration $[Q]$, f_a is the fraction of accessible fluorescence, and K_a is the effective quenching constant for the accessible fluorophores, which are analogous to associative binding constants for the quencher–acceptor system. The dependence of $F_0/\Delta F$ on the reciprocal value of quencher concentration $[Q]^{-1}$ is linear with the slope equal to the value of $(f_aK_a)^{-1}$. The value f_a^{-1} is fixed on the ordinate. The constant K_a is a quotient of the ordinate f_a^{-1} and the slope $(f_aK_a)^{-1}$. The Modified Stern–Volmer plots are shown in Fig. 2, and the calculated results are displayed in Table 3.

Table 3 Binding constants and sites of the compound **7a**–HSA system at pH = 7.4

	Modified Stern–Volmer method	Scatchard method			
T (K)	$10^{-4}K_a$ (L mol^{-1})	$10^{-4}K_b$ (L mol^{-1})	R	S.D.	n
294	4.03	4.15	0.994	0.009	1.44
302	3.74	3.79	0.998	0.004	1.39
310	3.51	3.57	0.997	0.005	1.38

When small molecules bind to a set of equivalent sites on a macromolecule, the equilibrium binding constants and the numbers of binding sites can also be calculated according to the Scatchard equation:[33]

$$r/D_f = nK_b - rK_b \quad (3)$$

where D_f is the molar concentration of free small molecules, r is the number of moles of small molecules bound per mole of protein, n is the binding sites multiplicity per class of binding site, and K_b is the equilibrium binding constant. The Scatchard plots are shown in Fig. 3 and the K_b and n are listed in Table 3.

Fig. 2 and 3 show the Modified Stern–Volmer and Scatchard plots for the compound **7a**–HSA system at different temperature. The decreasing trend of K_a and K_b with increasing temperature was in accordance with K_{SV}'s dependence on temperatures. The values of the binding sites n were approximately 1, which showed that one high affinity binding site was present in the interactions of compound **7a** with HSA. The results also showed that the binding constants were moderate and the effects of temperature were not significant, thus compound **7a** might be stored and carried by this protein.

3.2.4 Binding mode and thermodynamic parameters. Generally, there are four types of non-covalent interactions including hydrogen bonds, van der Waals forces, electrostatic and hydrophobic bonds, which play important roles in small molecules binding to proteins.[34] Changes in the thermodynamic parameters enthalpy (ΔH) and entropy (ΔS) during the

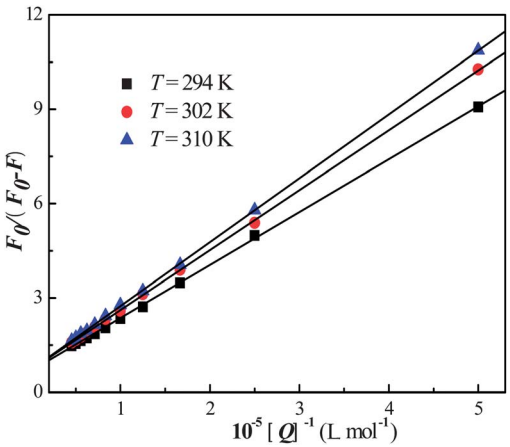

Fig. 2 Modified Stern–Volmer plots of the compound **7a**–HSA system at different temperatures.

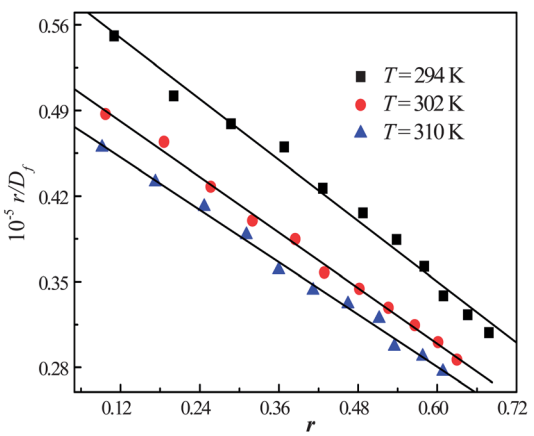

Fig. 3 Scatchard plots of the compound **7a**–HSA system at different temperatures.

binding reaction are the main evidence for the interactions between small molecules and proteins. If the enthalpy change (ΔH) does not vary significantly over the studied temperature range, then its value and that of entropy change (ΔS) can be evaluated from the van't Hoff equation:

$$\ln K = -\frac{\Delta H}{RT} + \frac{\Delta S}{R} \quad (4)$$

where K is analogous to the associative binding constants at the corresponding temperature and R is the gas constant. In order to explain the binding model between compound **7a** and HSA, the thermodynamic parameters were calculated from the van't Hoff plots. The enthalpy change (ΔH) was estimated from the slope of the van't Hoff relationship (Fig. S4, ESI 3†). The free energy change (ΔG) was then calculated from the following equation:

$$\Delta G = \Delta H - T\Delta S \quad (5)$$

Table 4 summarizes the values of ΔH, ΔG and ΔS. The negative values of the free energy ΔG of the interactions between compound **7a** and HSA suggest that the binding process is spontaneous, and the negative values of enthalpy (ΔH) indicate that the binding was mainly enthalpy-driven and involved an exothermic reaction, the entropy (ΔS) was unfavorable for it. A positive (ΔS) value is frequently taken as typical evidence for hydrophobic interactions, which was consistent with the above discussion. The negative (ΔH) value (-6.554 kJ mol^{-1}) observed cannot be mainly attributed to electrostatic interactions since electrostatic interactions ΔH were very small, almost zero.[35] Therefore, the enthalpy change $\Delta H < 0$ and the entropy change $\Delta S > 0$ obtained in this case indicate that the hydrophobic interactions and hydrogen bonds play an important role in the binding of compound **7a** to HSA,[30] electrostatic interactions might also be involved in the binding process.

3.2.5 Binding distance. A spectral overlap between the fluorescence spectrum of HSA and the UV-vis spectrum of compound **7a** is shown in Fig. 4. The salient overlap suggests that there is a direct resonance energy transfer between HSA and compound **7a**.

According to Förster's theory, the energy transfer efficiency (E) is defined by the following equation:[36]

$$E = 1 - \frac{F}{F_0} = \frac{R_0^6}{R_0^6 + r^6} \quad (6)$$

where E denotes the efficiency of transfer between the donor and the acceptor, r is the average distance between donor and acceptor, and R_0 is the Förster critical distance when the efficiency of transfer is 50%, F and F_0 are the fluorescence intensities of HSA in the presence and absence of compound **7a**, respectively. R_0 can be calculated from equation (7):

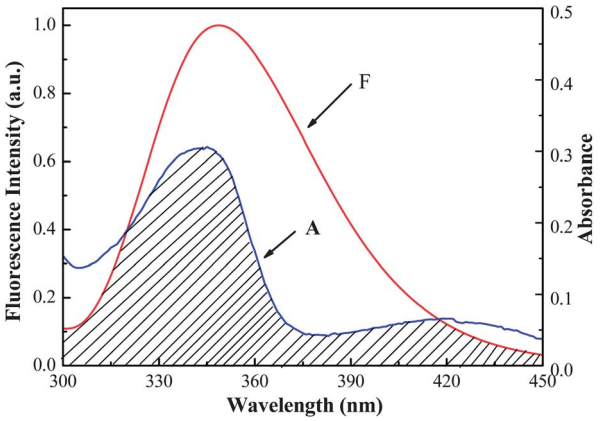

Fig. 4 Spectral overlap of compound **7a** absorption (curve A) with HSA fluorescence (curve F; T = 294 K). c(HSA) = c(compound **7a**) = 1.0 × 10^{-5} mol L^{-1}.

$$R_0^6 = 8.79 \times 10^{-25} K^2 n^{-4} \varphi J \quad (7)$$

where K^2 is the orientation factor related to the geometry of the donor (HSA) and acceptor (compound **7a**) of dipoles; n is the average refracted index of medium in the wavelength range where spectral overlap is significant; φ is the fluorescence quantum yield of the donor; J is the overlap integral of the emission spectrum of HSA and the absorption spectrum of compound **7a**, which could be obtained from equation (8):

$$J = \frac{\int_0^\infty F(\lambda)\varepsilon(\lambda)\lambda^4 \mathrm{d}\lambda}{\int_0^\infty F(\lambda)\mathrm{d}\lambda} \quad (8)$$

where $F(\lambda)$ is the fluorescence intensity of HSA in the wavelength range from λ to $\lambda + \Delta\lambda$, $\varepsilon(\lambda)$ is the extinction coefficient of compound **7a** at λ.

In the present case, $K^2 = 2/3$, $n = 1.36$, $\varphi = 0.074$,[37] according to equations (6)–(8), we calculated $J = 3.42 \times 10^{-14}$ cm^3 L mol^{-1}, $E = 0.385$, $R_0 = 2.75$ nm, and the binding distance $r = 2.97$ nm. The values for R_0 and r are on the 2–8 nm scale, and $0.5R_0 < r < 1.5R_0$, indicating the existence of interactions between compound **7a** and HSA.[38,39]

3.2.6 Molecular docking studies. HSA contains three homologous α-helical domains (I–III), each of which is composed of subdomains A and B. The principal regions of ligand binding sites in HSA are located in hydrophobic cavities in the subdomains IIA and IIIA.

Molecular docking evaluation was performed to understand the binding mode between compound **7a** and HSA. The docking mode with the lowest binding free energy (-11.32 kJ mol^{-1}) is shown in Fig. 5 and 6. As clearly evidenced, compound **7a** is surrounded by Arg-218, 257, Lys-195, 199, Leu-198, 238, 260, Ala-291, 455, Ile-264, 290, Asp-451, Phe-211 and Trp-214. Moreover, compound **7a** partly occupies subdomain IIA, resulting in fluorescence quenching of Trp-214. Hydrophobic

Table 4 Thermodynamic parameters of compound **7a**–HSA system at different temperatures

T (K)	ΔH (kJ mol^{-1})	ΔG (kJ mol^{-1})	ΔS (J mol^{-1} K^{-1})
294	−6.55	−25.92	65.86
302		−26.44	
310		−26.97	

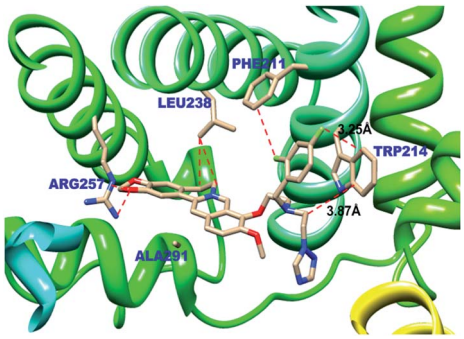

Fig. 5 Molecular docking of compound **7a** with HSA.

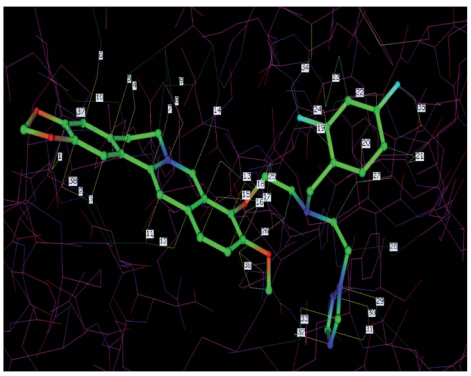

Fig. 6 Binding model of compound **7a** to HSA.

interactions exist between the aromatic ring of compound **7a** and Ile-264, 290, Leu-198, 238, 260, Ala-291, Lys-199 in HSA. Though the interactions are dominated by hydrophobic contacts, specific electrostatic interactions and hydrogen bonds between compound **7a** and Arg-257 in HSA are also involved in the binding process. All these indicate that the simulation results coincide well with the above thermodynamic analysis.

4 Conclusion

In summary, a series of berberine azoles was successfully synthesized through easy, convenient and economic synthetic procedures and their structures were confirmed by NMR, IR, MS and HRMS spectra. The *in vitro* antimicrobial evaluation showed that most of the synthesized berberine azoles effectively inhibit the growth of the tested strains. Particularly, berberine triazole **7a** gave excellent antimicrobial efficacies (MIC = 2 μg mL^{-1}) against *proteus vulgaris* and *candida mycoderma*, which are superior to the current clinical antimicrobial drugs. The binding investigations revealed that HSA can undergo fluorescent quenching in the presence of the prepared berberine triazole **7a** as a result of the formation of a ground-state compound **7a**–HSA complex. The calculated thermodynamic parameters indicate that the binding process is spontaneous, and that hydrogen bonds and hydrophobic interactions play important roles in the strong association of compound **7a** with HSA. Molecular docking experiments showed that compound **7a** has moderate affinity for HSA, and the theoretical calculations were in accordance with the experimental results.

Acknowledgements

This work was partially supported by the National Natural Science Foundation of China (no. 21172181), the Research Fellowship for International Young Scientists from International (Regional) Cooperation and Exchange Program (no. 81250110089, 81250110554), the key program from Natural Science Foundation of Chongqing (CSTC2012jjB10026) and the Specialized Research Fund for the Doctoral Program of Higher Education of China (SRFDP 20110182110007).

References

1 C. Q. Sheng, W. N. Zhang, H. T. Ji, M. Zhang, Y. L. Song, H. Xu, J. Zhu, Z. Y. Miao, Q. F. Jiang, J. Z. Yao, Y. J. Zhou, J. Zhu and J. G. Lu, *J. Med. Chem.*, 2006, **49**, 2512–2525.
2 C. Q. Sheng and W. N. Zhang, *Curr. Med. Chem.*, 2011, **18**, 733–766.
3 W. Y. Wang, S. Z. Wang, G. Q. Dong, Y. Liu, Z. Z. Guo, Z. Y. Miao, J. Z. Yao, W. N. Zhang and C. Q. Sheng, *Med. Chem. Commun.*, 2011, **2**, 1066–1072.
4 Y. Y. Zhang, J. L. Mi, C. H. Zhou and X. D. Zhou, *Eur. J. Med. Chem.*, 2011, **46**, 4391–4402.
5 V. S. Pore, M. A. Jagtap, S. G. Agalave, A. K. Pandey, M. I. Siddiqi, V. Kumar and P. K. Shukla, *Med. Chem. Commun.*, 2012, **3**, 484–488.
6 B. Fang, C. H. Zhou and X. C. Rao, *Eur. J. Med. Chem.*, 2010, **45**, 4388–4398.
7 X. L. Wang, K. Wan and C. H. Zhou, *Eur. J. Med. Chem.*, 2010, **45**, 4631–4639.
8 F. Turtaut, S. Ouahrani-Bettache, J. L. Montero, S. Köohler and J. Y. Winum, *Med. Chem. Commun.*, 2011, **2**, 995–1000.
9 S. L. Zhang, G. L. V. Damu, L. Zhang, R. X. Geng and C. H. Zhou, *Eur. J. Med. Chem.*, 2012, **55**, 164–175.
10 Y. Wang, G. L. V. Damu, J. S. Lv, R. X. Geng, D. C. Yang and C. H. Zhou, *Bioorg. Med. Chem. Lett.*, 2012, **22**, 5363–5366.
11 Y. S. Tong, J. J. Bouska, P. A. Ellis, E. F. Johnson, J. Leverson, X. S. Liu, P. A. Marcotte, A. M. Olson, D. J. Osterling, M. Przytulinska, L. E. Rodriguez, Y. Shi, N. Soni, J. Stavropoulos, S. Thomas, C. K. Donawho, D. J. Frost, Y. Luo, V. L. Giranda and T. D. Penning, *J. Med. Chem.*, 2009, **52**, 6803–6813.
12 W. S. Huang, C. A. Metcalf, R. Sundaramoorthi, Y. H. Wang, D. Zou, R. M. Thomas, X. T. Zhu, L. S. Cai, D. Wen, S. Y. Liu, J. Romero, J. W. Qi, I. Chen, G. Banda, S. P. Lentini, S. Das, Q. H. Xu, J. Keats, F. Wang, S. Wardwell, Y. Y. Ning, J. T. Snodgrass, M. I. Broudy, K. Russian, T. J. Zhou, L. Commodore, N. I. Narasimhan, Q. K. Mohemmad, J. Iuliucci, V. M. Rivera, D. C. Dalgarno, T. K. Sawyer, T. Clackson and W. C. Shakespeare, *J. Med. Chem.*, 2010, **53**, 4701–4719.
13 N. B. Patel, I. H. Khan and S. D. Rajani, *Eur. J. Med. Chem.*, 2010, **45**, 4293–4299.

14 Y. F. Li, G. F. Wang, P. L. He, W. G. Huang, F. H. Zhu, H. Y. Gao, W. Tang, Y. Luo, C. L. Feng, L. P. Shi, Y. D. Ren, W. Lu and J. P. Zuo, *J. Med. Chem.*, 2006, **49**, 4790–4794.
15 A. Ciupa, N. J. Griffiths, S. K. Light, P. J. Wood and L. Caggiano, *Med. Chem. Commun.*, 2011, **2**, 1011–1015.
16 N. Siddiqui and W. Ahsan, *Eur. J. Med. Chem.*, 2010, **45**, 1536–1543.
17 J. Valdez, R. Cedillo, A. Hernández-Campos, L. Yépez, F. Hernández-Luis, G. Navarrete-Vázquez, A. Tapia, R. Cortés, M. Hernández and R. Castillo, *Bioorg. Med. Chem. Lett.*, 2002, **12**, 2221–2224.
18 M. Berlin, C. W. Boyce and M. L. Ruiz, *J. Med. Chem.*, 2011, **54**, 26–53.
19 A. A. Siddiqui, R. Mishra, M. Shaharyar, A. Husain, M. Rashid and P. Pal, *Bioorg. Med. Chem. Lett.*, 2011, **21**, 1023–1026.
20 C. H. Zhou and Y. Wang, *Curr. Med. Chem.*, 2012, **19**, 239–280.
21 S. Samosorn, B. Tanwirat, N. Muhamad, G. Casadei, D. Tomkiewicz, K. Lewis, A. Suksamrarn, T. Prammananan, K. C. Gornall, J. L. Beck and J. B. Bremner, *Bioorg. Med. Chem.*, 2009, **17**, 3866–3872.
22 H. P. Kuo, T. C. Chuang, M. H. Yeh, S. C. Hsu, T. D. Way, P. Y. Chen, S. S. Wang, Y. H. Chang, M. C. Kao and J. Y. Liu, *J. Agric. Food Chem.*, 2011, **59**, 8216–8224.
23 H. S. Bodiwala, S. Sabde, D. Mitra, K. K. Bhutani and I. P. Singh, *Eur. J. Med. Chem.*, 2011, **46**, 1045–1049.
24 R. Gautam and S. M. Jachak, *Med. Res. Rev.*, 2009, **29**, 767–820.
25 M. Bahar, Y. Deng, X. Zhu, S. He, T. Pandharkar, M. E. Drew, A. Navarro-Vázquez, C. Anklin, R. R. Gil, R. W. Doskotch, K. A. Werbovetz and A. D. Kinghorn, *Bioorg. Med. Chem. Lett.*, 2011, **21**, 2606–2610.
26 J. L. Vennerstrom, J. K. Lovelace, V. B. Waits, W. L. Hanson and D. L. Klayman, *Antimicrob. Agents Chemother.*, 1990, **34**, 918–921.
27 F. Berti, S. Bincoletto, I. Donati, G. Fontanive, M. Fregonese and F. Benedetti, *Org. Biomol. Chem.*, 2011, **9**, 1987–1999.
28 Y. J. Hu, Y. Liu and X. H. Xiao, *Biomacromolecules*, 2009, **10**, 517–521.
29 D. C. Carter and J. X. Ho, *Adv. Protein Chem.*, 1994, **45**, 153–203.
30 V. D. Suryawanshi, P. V. Anbhule, A. H. Gore, S. R. Patil and G. B. Kolekar, *Ind. Eng. Chem. Res.*, 2012, **51**, 95–102.
31 J. R. Lakowicz, *Principles of Fluorescence Spectroscopy*, Springer, New York, 3rd edn, 2006, pp. 11–12.
32 S. S. Lehrer, *Biochemistry*, 1971, **10**, 3254–3263.
33 G. Scatchard, *Ann. N. Y. Acad. Sci.*, 1949, **51**, 660–672.
34 U. S. Mote, S. R. Patil, S. H. Bhosale, S. H. Han and G. B. Kolekar, *J. Photochem. Photobiol., B*, 2011, **103**, 16–21.
35 D. P. Ross and S. Subramanian, *Biochemistry*, 1981, **20**, 3096–3102.
36 J. R. Lakowicz, G. Piszczek and J. S. Kang, *Anal. Biochem.*, 2001, **288**, 62–75.
37 L. Cyril, J. K. Earl and W. M. Sperry, *Biochemists' handbook*, E. & F.N. Spon, London, 1961, pp. 83–85.
38 J. Y. Yang and W. Y. Yang, *J. Am. Chem. Soc.*, 2009, **131**, 11644–11645.
39 B. Valeur, *Molecular Fluorescence: principles and applications*, Wiley, New York, 2001, pp. 247–272.

